

Multipiezo effect in altermagnetic V₂SeTeO monolayer

Yu Zhu,^{1ξ} Taikang Chen,^{1ξ} Yongchang Li,¹ Lei Qiao,¹ Xiaonan Ma,¹ Tao Hu,² Heng

Gao,^{1*} and Wei Ren^{1,3‡}

¹Department of Physics, Shanghai Key Laboratory of High Temperature Superconductors, International Centre of Quantum and Molecular Structures, Shanghai University, Shanghai 200444, China

²School of Materials Science and Engineering, Shanghai University, Shanghai 200444, China

³Zhejiang Laboratory, Hangzhou 311100, China

[*gaoheng@shu.edu.cn](mailto:gaoheng@shu.edu.cn) [‡renwei@shu.edu.cn](mailto:renwei@shu.edu.cn)

^ξThese authors contributed equally to this work.

Inspired by recent theoretical proposal on the interesting piezomagnetism and C-paired valley polarization in V₂Se₂O monolayer, we predict a stable antiferromagnetic Janus monolayer V₂SeTeO with altermagnetic configuration using density functional theory calculations. It exhibits a novel “multi-piezo” effect combining piezoelectric, piezovally and piezomagnetism. Most interestingly, the valley polarization and the net magnetization under strain in V₂SeTeO exceed these in V₂Se₂O, along with the additional large piezoelectric coefficient of e_{31} (0.322×10^{-10} C/m). The “multi-piezo” effect makes antiferromagnetic Janus monolayer V₂SeTeO a tantalizing material for potential applications in nanoelectronics, optoelectronics, spintronics and valleytronics.

I. INTRODUCTION

The pursuit of miniaturization for multifunctional electronic devices necessitates exploring new degrees of freedom and approaches to integrate and manipulate multiple functions in nanoscale materials [1-5]. The exfoliation of graphene in 2004 [6] sparked tremendous interest in two-dimensional (2D) materials such as boronene [7,8], phosphene [9,10], and monochalcogenides [11], which can be exfoliated into monolayers possessing unique properties for quantum devices. Multiferroics, materials exhibiting coupled two or more ferroic orders (i.e., ferroelectric, ferromagnetic, and ferroelastic), are particularly interesting for next-generation of electronics [12-16]. However, stabilizing multiple ferroic orders in a 2D material remains challenging [17]. Thus, whether there are other alternatives to achieve the purpose of multifunctional nanomaterials?

Strain engineering provides a potential method for tuning and enriching physical properties thanks to the high stretchability of nanomaterials [18-20]. Under mechanical strain, nanomaterials exhibit interesting responses including piezoelectricity, piezoluminescence and piezomagnetism. Piezoelectricity is a well-known phenomenon of electromechanical coupling that can generate voltage under mechanical strain [21,22]. Piezoluminescence refers to light emission during elastic deformation [23,24]. Piezomagnetism occurs in some antiferromagnetic (AFM) crystals, where applied external stress induces ferromagnetic moment [25-27]. In contrast to conventional ferrovalley materials requiring time-reversal symmetry, recent works showed valleys in altermagnetic V_2Se_2O [28] monolayer are found to be protected by crystal symmetry and coined C-paired spin-valley-locking (SVL). Applying uniaxial strain generates valley polarization, known as piezovally effect. Additionally, Doping V_2Se_2O can also induce piezomagnetism [28]. An intriguing question is whether piezoelectricity can be introduced into V_2Se_2O while retaining the multi-piezo effect? Recent interest in 2D Janus structures [29-32] provides an opportunity, since they exhibit intrinsic mirror symmetry breaking that enables out-of-plane piezoelectric.

In our work, motivated by recent experimental progress in the synthesis of Janus monolayers [33,34] (MoSSe, for example) and bulk V_2Se_2O [35], along with theoretical studies of V_2Se_2O monolayer [28], we designed a Janus V_2SeTeO monolayer. It naturally exhibits broken out-of-plane symmetry and intact in-plane symmetry, enabling large out-of-plane piezoelectricity while preserving the original in-plane properties. A novel multi-piezo effect combining piezovolley polarization, piezomagnetism and piezoelectricity is realized in the Janus V_2SeTeO monolayer. Remarkably, these three mechanical responses are not causally related to each other, not as the phenomenon of magneto-electric coupling in multiferroics does. The modulation methods and mechanisms of these three piezo-effects are independent of each other, with piezoelectricity being out-of-plane, piezovolley and piezomagnetism being protected by in-plane symmetry. A ferromagnetic moment only arises upon doping the strained V_2SeTeO . Our discovery of the multi-piezo effect provides a new direction and theoretical guidance for designing multifunctional nanodevices which couple electrical, chemical and magnetic controls through external mechanical strain.

II. COMPUTATIONAL METHODS

We performed calculations on the basis of density functional theory (DFT) by employing the Vienna ab initio simulation package (VASP) [36,37], and the projected augmented wave (PAW) method [38]. The cutoff energy for plane-wave expansion was set to be 600 eV. Regarding the exchange-correlation functional, the generalized gradient approximation (GGA) of the Perdew-Burke-Ernzerh was adopted [39]. The optB88b-vdW method was employed for van der Waals (vdW) correction during the structure optimization [40,41]. V-3d electron localization [42] was treated with GGA+U approach [43] using $U = 4$ eV, consistent with previous reports [44-46]. The crystal structure was fully relaxed with the convergence criteria for the total energy and force, which were set to be 10^{-8} eV and 0.005 eV/Å, respectively. The Monkhorst-Pack k-points were sampled in the 2D Brillouin zone using a Γ -centered $10 \times 10 \times 1$ k-grid. To avoid interlayer interactions, a vacuum layer of 25 Å is placed along the c-axis. The ab initio molecular dynamics (AIMD) simulations [47] were

carried out using $5 \times 5 \times 1$ supercell at 300 K with a 1 fs time step. The phonon dispersion spectrum using density-functional perturbation theory (DFPT) with a $4 \times 4 \times 1$ supercell was calculated to verify the dynamic stability using the PHONOPY code [48,49].

III. RESULTS AND DISCUSSIONS

A . Geometric and altermagnetism

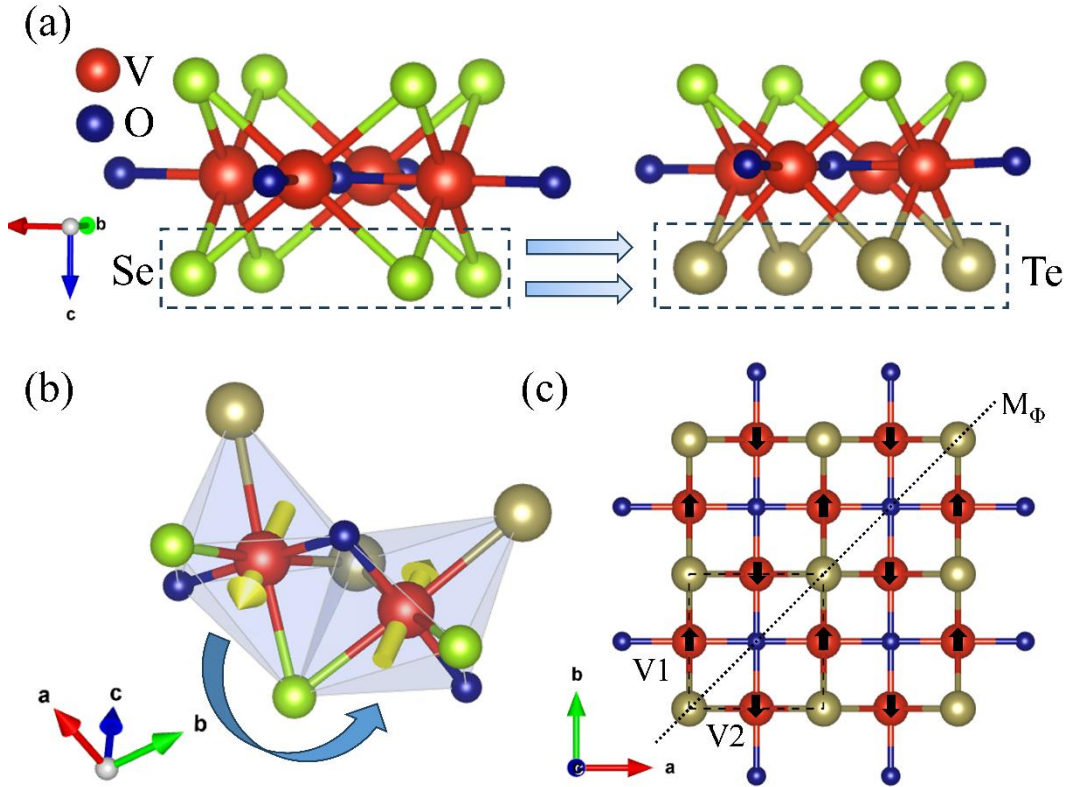


Figure 1 (a) Schematic diagram of the element substitution from V_2Se_2O monolayer to Janus V_2SeTeO monolayer. (b) Altermagnetic structure of V_2SeTeO monolayer, where the yellow arrows directions indicate the spin alignment on the sublattice of the two V atoms. (c) The 2D Neel AFM order has magnetic moments located on the V1 and V2 atoms (black arrows). The dotted line shows the primitive cell. M_Φ denotes diagonal mirror symmetry in the ab plane.

V_2Se_2O monolayer is a three-layer atomic structure sandwiched by two Se planes [28]. Substituting Se with Te in the bottom layer of V_2Se_2O creates the Janus V_2SeTeO monolayer, as depicted in Figure 1 (a). Compared to V_2Se_2O monolayer (space group number 123, $P4/mmm$), Janus V_2SeTeO monolayer (space group

number 99, P4mm) exhibits lower symmetry due to out-of-plane mirror symmetry breaking while retaining the tetragonal structure and in-plane C_{4v} symmetry. The calculated structural parameters including lattice constants, bond lengths and bond angles for both V_2Se_2O and V_2SeTeO monolayers are listed in [Table S1](#). The length of the V-Se bond is shorter than that of the V-Te bond and the angles between Se-V-Se and Te-V-Te are different, while the anisotropic bonding shears the structure and reduces its symmetry. The V_2SeTeO primitive cell contains two V atoms, and each of them is coordinated by two Se atoms, two Te atoms, and two oxygen atoms in a highly distorted octahedral structure in [Figure 1 \(b\)](#), possessing $\sim 2 \mu_B$ local magnetic moments. This indicates that the Janus structure primarily impacts on the symmetry without significantly changing the magnetic properties. The in-plane diagonal mirror symmetry M_Φ is preserved, changing from the Se-O-Se to Se/Te-O-Se/Te plane as shown in [Figure 1 \(c\)](#).

Four magnetic configurations of a $2 \times 2 \times 1$ Janus V_2SeTeO supercell ([Figure S1](#)) were constructed and calculated to determine the magnetic ground state. AFM-Neel configuration ([Figure 1 \(c\)](#)) is the most stable, with energy differences listed in Table I, confirming the intrinsic antiferromagnetism akin to V_2Se_2O . Interestingly, this AFM Neel state exhibits the recently defined altermagnetism [50,51], enabling spin splitting in conventional collinear antiferromagnets. To better characterize the magnetic properties, the calculated magnetic anisotropy energy (MAE) is found to be $143 \mu eV/\text{unit cell}$, with the magnetic easy-axis along the diagonal of the ab plane.

[Figure S2 \(a\)](#) presents the calculated phonon spectrum for the V_2SeTeO monolayer and there is no obvious imaginary frequency, which confirms the structural stability. The thermal stability of Janus V_2SeTeO was also verified through *ab initio* molecular dynamics with only slight energy fluctuations during the simulations ([Figure S2 \(b\)](#)). The elastic constants ([Table S2](#)) satisfy the Born criteria [52]: $C_{11} > 0$, $C_{66} > 0$, and $C_{11} > |C_{12}|$ indicating the mechanical stability of V_2SeTeO monolayer. In summary, these results demonstrate the intrinsic stability of the Janus V_2SeTeO monolayer in the AFM ground state.

B. Electronic properties and piezovolley

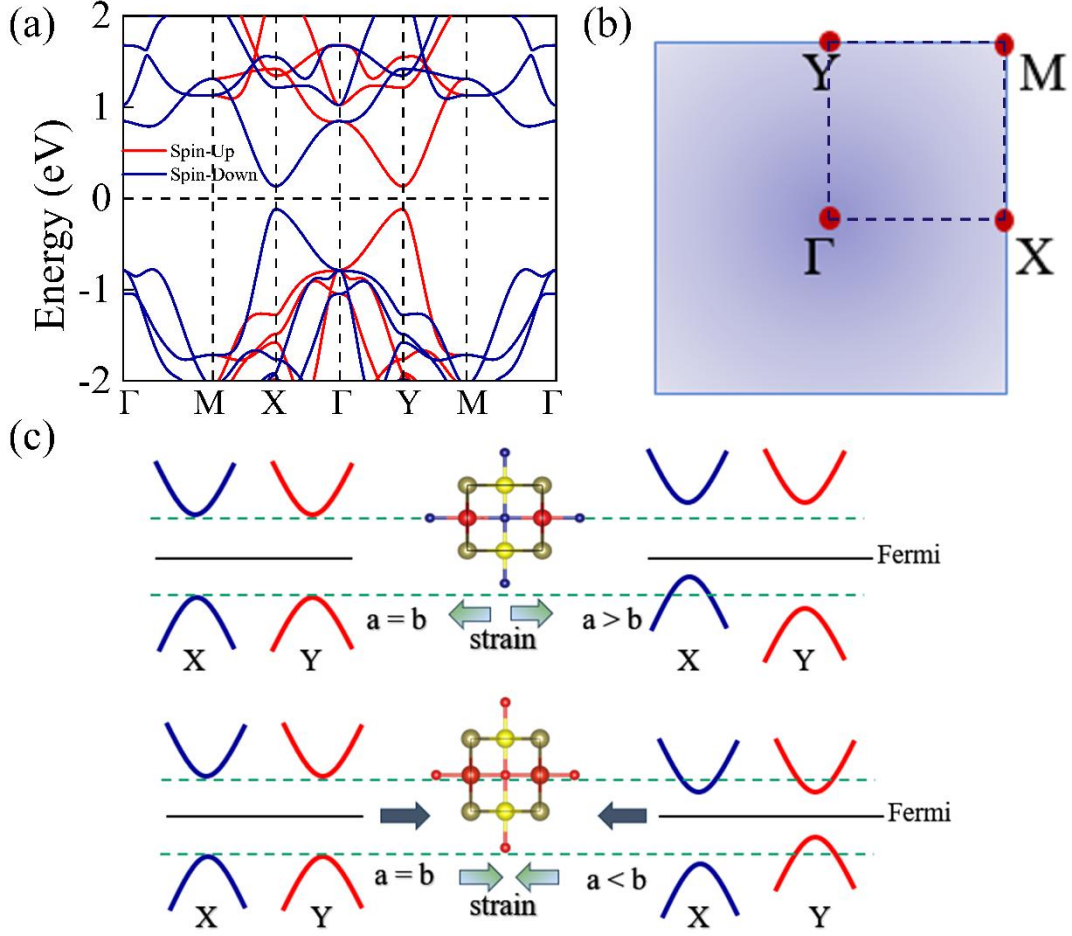


Figure 2 (a) Spin-resolved electronic band structure of Janus V_2SeTeO monolayer, with spin-up (red lines) and spin-down (blue lines) channels. (b) The first Brillouin zone with high symmetry points. (c) Schematic of the piezovolley mechanism, the blue and red lines indicate the valleys at points X and Y, respectively.

The band structure and density of states (DOS) of V_2SeTeO monolayer are shown in [Figure 2 \(a\)](#) and [Figure S3](#) by GGA+U method without spin-orbital coupling (SOC). The Brillouin zone for band structure calculations is shown in [Figure 2 \(b\)](#), which is related to the crystal structure. It turns out that the V_2SeTeO monolayer is a semiconductor with a 0.25 eV direct band gap, smaller than the value 0.72 eV of V_2Se_2O [28], owing to the more metallic nature of Te versus Se. Notably, the band structure in [Figure 2 \(a\)](#) exhibits clear spin-splitting, distinct from conventional AFM materials. This arises from its altermagnetic order shown in [Figure 1 \(b\)-\(c\)](#), which breaks both PT symmetry (the combination of spatial inversion P and time reversal T symmetries) and UL symmetry (the combination of spinor U and translation L symmetries) to allow spin splitting with or without SOC [53]. (See [Note S1](#) for the

detailed symmetry rules). Altermagnetism has also been reported in many known materials, like bulk oxide MnO_2 [54] and RuO_2 [55,56], perovskite oxide insulators LaMnO_3 [57,58] and CaCrO_3 [59], 2D materials $\text{V}_2\text{Se}_2\text{O}$ [28] and CrO [60]. As shown in Figure 1 (b)-(c), in the alternating magnetic configuration, the magnetic V atoms with different spin directions cannot be related by pure translation due to differing spin directions, requiring instead rotation operations that break symmetry and induce spin polarization. Exploiting this feature of altermagnetism may overcome the inability for spin polarization in AFMs, better enabling spintronic applications.

Previous works on $\text{V}_2\text{Se}_2\text{O}$ [28] showed uniaxial strain can produce valley polarization in the altermagnetic structure. Similarly, degenerate band valleys are observed at X and Y points in V_2SeTeO (Figure 2 (a)), contributed by V atoms with different spin alignments. This exemplifies the SVL, lock-coupling the spin and valley degrees of freedom. Valley traditionally arises in transition metal dichalcogenides (TMDs) via ferrovalley ordering, requiring strong SOC, broken inversion symmetry and heavy elements [61-63]. Uniquely here, valleys in V_2SeTeO are protected by the mirror symmetry rather than the time-reversal symmetry. This relaxes the constraints for realizing valley polarization, providing new avenues to design valleytronics materials.

As in $\text{V}_2\text{Se}_2\text{O}$, in-plane uniaxial strain along the a/b axis breaks the mirror symmetry and generates a valley polarization which we term the “piezovally effect”. The physical mechanism of piezovally can be seen in Figure 2 (c). The valley energies $E(X)$ and $E(Y)$ at X and Y are no longer degenerate, thus the valley polarization can be defined as the energy difference between two valleys $P=E(X)-E(Y)$. The valley polarization of valence and conduction bands versus uniaxial strain along a direction is shown in Figure 3 (a). It turns out that the valley polarization changes monotonously under the control of strain, with opposite trends along the a and b directions due to the diagonal mirror symmetry M_Φ . Remarkably, the valley polarization of 128 meV induced by 4% tensile strain exceeds reported values in 2D ferrovalley materials such as LaBrI (59 meV) [64], 2H-FeCl_2 (101 meV) [65], VSCl

(57.8 meV) [66], and VSSe (85 meV) [67], and also larger than ~ 60 meV in V_2Se_2O [28]. As for electronic properties, the band structures of V_2SeTeO under uniaxial strain from -4% to 4% are plotted in Figure S4, as well as band gap variation (two valleys' band gaps [X and Y] and overall gap [total]) in Figure 3 (b). These results indicate that the predicted Janus V_2SeTeO monolayer retains altermagnetic structure and realize notably enhanced piezovoltage under strain.

C. Piezomagnetism

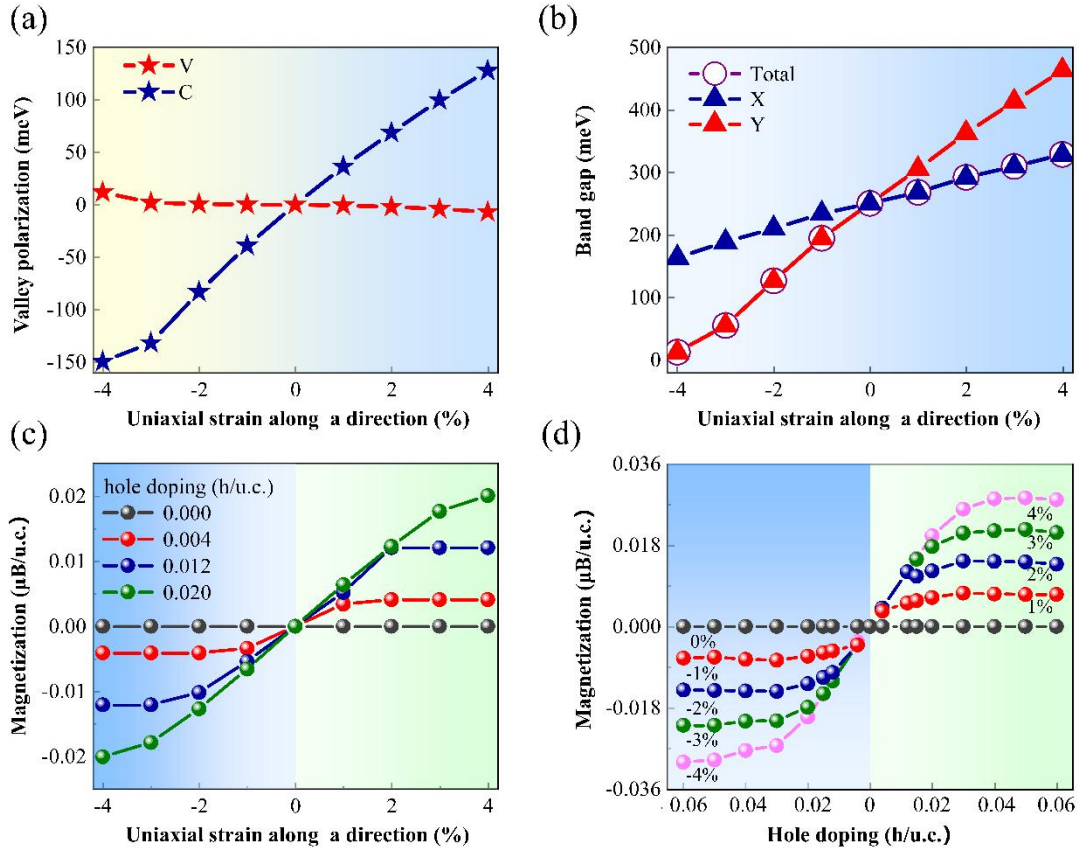


Figure 3 The strain-controlled (a) valley polarization generated at the valence band [V] and the conduction band [C], (b) valley gaps at X and Y, as well as the total bandgap, and (c)-(d) the corresponding net magnetization per unit cell for different concentration of hole doping.

Strain induced valley polarization in V_2SeTeO monolayer enables new opportunities to generate net magnetic moments. Magnetism depends on integrating the spin density within the energy range from negative infinity to the Fermi level. Tuning the Fermi level to cross only one valley through carrier doping or gating can

produce net moments. This is expressed as $M = \int_{-\infty}^{E_f^{(n)}} [\rho^\uparrow(\varepsilon) - \rho^\downarrow(\varepsilon)] dE$, where E_f is the doped Fermi level, n is the doping density, and $\rho^{\uparrow(\downarrow)}$ represents the spin-up (spin-down) part of the DOS under external strain ε [28].

Without doping, no net magnetic moment arises in the strained V_2SeTeO , consistent with the undoped band structure as shown in Figure S4. Under certain doping concentration, the magnetization increases continuously with uniaxial strain, with opposite magnetic directions induced by tensile and compressive strains. The higher doping concentrations generally produce the greater magnetization under a certain strain. The magnetization shows an initial linear response under the small strain, and eventually saturating under large strains. The higher doping concentration also leads to the higher magnetization saturation as shown in Figure 3 (c)-(d). Doping-dependent band structure of V_2SeTeO as a function of uniaxial strain in Figure S5, indicating the variation of magnetization polarization. Unlike noncollinear cases, piezomagnetism is rarely reported in antiferromagnets. The unique altermagnetic structure and low magnetocrystalline anisotropy of V_2SeTeO enable controlling the magnetic direction and moments through various means of electric field and doping.

D. Piezoelectricity in Janus V_2SeTeO monolayer

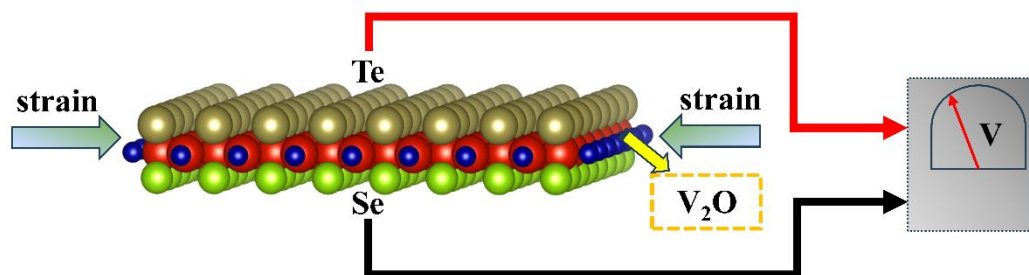


Figure 4 Schematic diagram of the mechanism for the generation of the out-of-plane piezoelectric parameter e_{31} , derived from the Janus structure of V_2SeTeO .

Piezoelectricity arises in noncentrosymmetric semiconductors, presenting electrical polarization under mechanical strain that enables electromechanical coupling. The centrosymmetric V_2Se_2O monolayer lacks piezoelectricity [28], but Janus structures can introduce large out-of-plane piezoelectricity by breaking the

horizontal mirror symmetry [29-32]. Substituting Se atoms in bottom layer with Te atoms breaks the horizontal mirror symmetry and induces an out-of-plane piezoelectricity in V_2SeTeO as shown in Figure 4. The piezoelectric tensor $e_{ijk} = \partial P_i / \partial \varepsilon_{jk}$ relates polarization P_i to the strain ε_{jk} , where i, j, k denote the x, y, z Cartesian directions. This third-rank tensor characterizes the piezoelectric response [68].

Symmetry analysis indicates that the Janus V_2SeTeO monolayer (point group C_{4v}) has only one independent piezoelectric component e_{31} ($e_{32} = e_{31}$). A large e_{31} of 0.322×10^{-10} C/m is obtained by the DFPT method, comprising opposite electronic (0.365×10^{-10} C/m) and ionic (-0.043×10^{-10} C/m) contributions, with the electronic part dominating. The value of e_{31} in V_2SeTeO represents a significantly enhanced out-of-plane piezoelectricity, compared to materials like WSSe ($e_{31} = 0.018 \times 10^{-10}$ C/m) and WSeTe ($e_{31} = 0.010 \times 10^{-10}$ C/m) monolayers [32], MoSTe multilayer ($e_{31} = 0.119 \times 10^{-10}$ C/m) [32], GdClF monolayer ($e_{31} = -0.181 \times 10^{-10}$ C/m) [69], In_2SSe monolayer ($e_{31} = 0.130 \times 10^{-10}$ C/m) [70]. The giant vertical piezoelectric polarization is expected to enable multifunctional piezoelectric applications for Janus V_2SeTeO .

IV. CONCLUSIONS

In conclusion, by means of first principles calculations we predict a novel Janus V_2SeTeO 2D monolayer with high dynamic and mechanical stabilities. The broken out-of-plane symmetry alongside maintained in-plane symmetry in Janus V_2SeTeO monolayer induces giant out-of-plane piezoelectricity while preserving original in-plane properties. This enables a remarkable multi-piezo effect combining piezovolley, piezomagnetism and piezoelectricity. Moreover, the large piezoelectric coefficient of 0.322×10^{-10} C/m is found, and the valley-polarization and net magnetization of V_2SeTeO are larger than V_2Se_2O . Significantly, these three mechanical responses do not causally influence each other, and they are protected by different mechanisms and are modulated relatively independently, with piezoelectricity being out-of-plane, piezovolley and piezomagnetism being protected by in-plane symmetry, while the net magnetic moment is only present upon doping in the uniaxially strained V_2SeTeO . Our work reveals an exciting new quantum mechanical phenomenon - the multipiezo

effect in a 2D Janus material. The integration of electrical, magnetic and chemical control through strain provides advantages for next-generation multifunctional nanoelectronics.

ACKNOWLEDGEMENTS

This work was supported by National Natural Science Foundation of China (12074241, 11929401, 52120204), Science and Technology Commission of Shanghai Municipality (22XD1400900, 20501130600, 21JC1402700, 21JC1402600, 22YF1413300), China Postdoctoral Science Foundation (2022M722035), Key Research Project of Zhejiang Laboratory (2021PE0AC02), Shanghai Technical Service Center of Science and Engineering Computing, Shanghai University.

DECLARATION OF COMPETING INTEREST

The authors declare that they have no known competing financial interests or personal relationships that could have appeared to influence the work reported in this paper.

SUPPLEMENTARY MATERIAL

See the supplementary material for more details of the studied V_2SeTeO monolayer.

REFERENCE

- [1] H. He, L. Guan, H. Le Ferrand, Controlled local orientation of 2D nanomaterials in 3D devices: methods and prospects for multifunctional designs and enhanced performance, *Journal of Materials Chemistry A* 10 (2022) 19129-19168.
- [2] N. A. Spaldin, W. E. Pickett, Computational design of multifunctional materials, *Journal of Solid State Chemistry* 176 (2003) 615-632.
- [3] G. Pacchioni, Two-dimensional oxides: Multifunctional materials for advanced technologies, *Chemistry—A European Journal* 18 (2012) 10144-10158.
- [4] L. Christodoulou, J. D. Venables, Multifunctional material systems: The first generation, *Jom* 55 (2003) 39-45.
- [5] J. P. Thomas, M. A. Qidwai, Mechanical design and performance of composite multifunctional materials, *Acta materialia* 52 (2004) 2155-2164.
- [6] K. S. Novoselov, A. K. Geim, S. V. Morozov, D.-e. Jiang, Y. Zhang, S. V. Dubonos, I. V. Grigorieva, A. A. Firsov, Electric field effect in atomically thin carbon films, *science* 306 (2004)

666-669.

- [7] B. Feng, J. Zhang, Q. Zhong, W. Li, S. Li, H. Li, P. Cheng, S. Meng, L. Chen, K. Wu, Experimental realization of two-dimensional boron sheets, *Nature chemistry* 8 (2016) 563-568.
- [8] A. J. Mannix, X.-F. Zhou, B. Kiraly, J. D. Wood, D. Alducin, B. D. Myers, X. Liu, B. L. Fisher, U. Santiago, J. R. Guest, Synthesis of borophenes: Anisotropic, two-dimensional boron polymorphs, *Science* 350 (2015) 1513-1516.
- [9] L. Kou, C. Chen, S. C. Smith, Phosphorene: fabrication, properties, and applications, *The journal of physical chemistry letters* 6 (2015) 2794-2805.
- [10] K. Cho, J. Yang, Y. Lu, Phosphorene: An emerging 2D material, *Journal of Materials Research* 32 (2017) 2839-2847.
- [11] L. Li, M. Wu, Binary compound bilayer and multilayer with vertical polarizations: two-dimensional ferroelectrics, multiferroics, and nanogenerators, *ACS nano* 11 (2017) 6382-6388.
- [12] C. A. F. Vaz, U. Staub, Artificial multiferroic heterostructures, *Journal of Materials Chemistry C* 1 (2013) 6731-6742.
- [13] J. S. Andrew, J. D. Starr, M. A. Budi, Prospects for nanostructured multiferroic composite materials, *Scripta Materialia* 74 (2014) 38-43.
- [14] S. Picozzi, C. Ederer, First principles studies of multiferroic materials, *Journal of Physics: Condensed Matter* 21 (2009) 303201.
- [15] J. Scott, Multiferroic memories, *Nature materials* 6 (2007) 256-257.
- [16] W. Eerenstein, N. Mathur, J. F. Scott, Multiferroic and magnetoelectric materials, *nature* 442 (2006) 759-765.
- [17] R. Qiu, Theoretical investigation of ferroic instabilities in confined geometries and distorted lattices, (2017).
- [18] S. Yang, Y. Chen, C. Jiang, Strain engineering of two-dimensional materials: methods, properties, and applications, *InfoMat* 3 (2021) 397-420.
- [19] Y. Sun, K. Liu, Strain engineering in functional 2-dimensional materials, *Journal of Applied Physics* 125 (2019).
- [20] R. Roldán, A. Castellanos-Gomez, E. Cappelluti, F. Guinea, Strain engineering in semiconducting two-dimensional crystals, *Journal of Physics: Condensed Matter* 27 (2015) 313201.
- [21] P. C. Sherrell, M. Fronzi, N. A. Shepelin, A. Corletto, D. A. Winkler, M. Ford, J. G. Shapter, A. V. Ellis, A bright future for engineering piezoelectric 2D crystals, *Chemical Society Reviews* 51 (2022) 650-671.
- [22] M. N. Blonsky, H. L. Zhuang, A. K. Singh, R. G. Hennig, Ab initio prediction of piezoelectricity in two-dimensional materials, *ACS nano* 9 (2015) 9885-9891.
- [23] D. Tu, C. N. Xu, S. Kamimura, Y. Horibe, H. Oshiro, L. Zhang, Y. Ishii, K. Hyodo, G. Marriott, N. Ueno, Ferroelectric Sr₃Sn₂O₇: Nd³⁺: a new multipiezo material with ultrasensitive and sustainable near-infrared piezoluminescence, *Advanced Materials* 32 (2020) 1908083.
- [24] D. Tu, C. N. Xu, A. Yoshida, M. Fujihala, J. Hirotsu, X. G. Zheng, LiNbO₃: Pr³⁺: a multipiezo material with simultaneous piezoelectricity and sensitive piezoluminescence, *Advanced Materials* 29 (2017) 1606914.
- [25] D. Boldrin, A. P. Mihai, B. Zou, J. Zemen, R. Thompson, E. Ware, B. V. Neamtu, L. Ghivelder, B. Esser, D. W. McComb, Giant piezomagnetism in Mn₃NiN, *ACS applied materials & interfaces* 10 (2018) 18863-18868.

- [26] T. Moriya, Piezomagnetism in CoF₂, *Journal of Physics and Chemistry of Solids* 11 (1959) 73-77.
- [27] A. Borovik-Romanov, H. Grimmer, M. Kenzelmann, *Piezomagnetism*, (2013).
- [28] H.-Y. Ma, M. Hu, N. Li, J. Liu, W. Yao, J.-F. Jia, J. Liu, Multifunctional antiferromagnetic materials with giant piezomagnetism and noncollinear spin current, *Nature communications* 12 (2021) 2846.
- [29] X. Tang, L. Kou, 2D Janus transition metal dichalcogenides: Properties and applications, *physica status solidi (b)* 259 (2022) 2100562.
- [30] X. Zhang, Y. Cui, L. Sun, M. Li, J. Du, Y. Huang, Stabilities, and electronic and piezoelectric properties of two-dimensional tin dichalcogenide derived Janus monolayers, *Journal of Materials Chemistry C* 7 (2019) 13203-13210.
- [31] J. Qiu, H. Li, X. Chen, B. Zhu, H. Guo, F. Zhang, Z. Ding, L. Lang, J. Yu, J. Bao, Piezoelectricity of Janus Sb₂Se₂Te monolayers: A first-principles study, *Journal of Applied Physics* 129 (2021) 125109.
- [32] L. Dong, J. Lou, V. B. Shenoy, Large in-plane and vertical piezoelectricity in Janus transition metal dichalcogenides, *ACS nano* 11 (2017) 8242-8248.
- [33] J. Zhang, S. Jia, I. Kholmanov, L. Dong, D. Er, W. Chen, H. Guo, Z. Jin, V. B. Shenoy, L. Shi, Janus monolayer transition-metal dichalcogenides, *ACS nano* 11 (2017) 8192-8198.
- [34] A.-Y. Lu, H. Zhu, J. Xiao, C.-P. Chuu, Y. Han, M.-H. Chiu, C.-C. Cheng, C.-W. Yang, K.-H. Wei, Y. Yang, Janus monolayers of transition metal dichalcogenides, *Nature nanotechnology* 12 (2017) 744-749.
- [35] H. Lin, J. Si, X. Zhu, K. Cai, H. Li, L. Kong, X. Yu, H.-H. Wen, Structure and physical properties of CsV₂Se_{2-x}O and V₂Se₂O, *Physical Review B* 98 (2018) 075132.
- [36] G. Kresse, J. Furthmüller, Efficient iterative schemes for ab initio total-energy calculations using a plane-wave basis set, *Physical review B* 54 (1996) 11169.
- [37] G. Kresse, J. Furthmüller, Efficiency of ab-initio total energy calculations for metals and semiconductors using a plane-wave basis set, *Computational materials science* 6 (1996) 15-50.
- [38] P. E. Blöchl, Projector augmented-wave method, *Physical review B* 50 (1994) 17953.
- [39] J. P. Perdew, K. Burke, M. Ernzerhof, Generalized gradient approximation made simple, *Physical review letters* 77 (1996) 3865.
- [40] M. Dion, H. Rydberg, E. Schröder, D. C. Langreth, B. I. Lundqvist, Van der Waals density functional for general geometries, *Physical review letters* 92 (2004) 246401.
- [41] J. Klimeš, D. R. Bowler, A. Michaelides, Van der Waals density functionals applied to solids, *Physical Review B* 83 (2011) 195131.
- [42] A. Liechtenstein, V. I. Anisimov, J. Zaanen, Density-functional theory and strong interactions: Orbital ordering in Mott-Hubbard insulators, *Physical Review B* 52 (1995) R5467.
- [43] S. L. Dudarev, G. A. Botton, S. Y. Savrasov, C. Humphreys, A. P. Sutton, Electron-energy-loss spectra and the structural stability of nickel oxide: An LSDA+ U study, *Physical Review B* 57 (1998) 1505.
- [44] X. Cheng, S. Xu, F. Jia, G. Zhao, M. Hu, W. Wu, W. Ren, Intrinsic ferromagnetism with high Curie temperature and strong anisotropy in a ferroelastic VX monolayer (X= P, As), *Physical Review B* 104 (2021) 104417.
- [45] X. Gao, R. Lian, L. He, Q. Fu, S. Indris, B. Schwarz, X. Wang, G. Chen, H. Ehrenberg, Y. Wei, Phase transformation, charge transfer, and ionic diffusion of Na₄MnV(PO₄)₃ in sodium-ion

batteries: a combined first-principles and experimental study, *Journal of Materials Chemistry A* 8 (2020) 17477-17486.

[46] J. Xing, H. Cao, A. Paul, C. Hu, H.-H. Wang, Y. Luo, R. Chaklashiya, J. M. Allred, S. Brown, T. Birol, Anisotropic properties, charge ordering, and ferrimagnetic structures in the strongly correlated β - V_2PO_5 single crystal, *Physical Review Materials* 4 (2020) 094414.

[47] S. Nosé, A unified formulation of the constant temperature molecular dynamics methods, *The Journal of chemical physics* 81 (1984) 511-519.

[48] A. Togo, F. Oba, I. Tanaka, First-principles calculations of the ferroelastic transition between rutile-type and $CaCl_2$ -type SiO_2 at high pressures, *Physical Review B* 78 (2008) 134106.

[49] A. Togo, I. Tanaka, First principles phonon calculations in materials science, *Scripta Materialia* 108 (2015) 1-5.

[50] L. Šmejkal, J. Sinova, T. Jungwirth, Emerging research landscape of altermagnetism, *Physical Review X* 12 (2022) 040501.

[51] I. Turek, Altermagnetism and magnetic groups with pseudoscalar electron spin, *Physical Review B* 106 (2022) 094432.

[52] R. C. Andrew, R. E. Mapasha, A. M. Ukpong, N. Chetty, Mechanical properties of graphene and boronitrene, *Physical review B* 85 (2012) 125428.

[53] L.-D. Yuan, Z. Wang, J.-W. Luo, E. I. Rashba, A. Zunger, Giant momentum-dependent spin splitting in centrosymmetric low-Z antiferromagnets, *Physical Review B* 102.1 (2020) 014422.

[54] Y. Noda, K. Ohno, S. Nakamura, Momentum-dependent band spin splitting in semiconducting MnO_2 : a density functional calculation, *Physical Chemistry Chemical Physics* 18 (2016) 13294-13303.

[55] K.-H. Ahn, A. Hariki, K.-W. Lee, J. Kuneš, Antiferromagnetism in RuO_2 as d-wave Pomeranchuk instability, *Physical Review B* 99 (2019) 184432.

[56] L. Šmejkal, R. González-Hernández, T. Jungwirth, J. Sinova, Crystal time-reversal symmetry breaking and spontaneous Hall effect in collinear antiferromagnets, *Science advances* 6 (2020) eaaz8809.

[57] T. Okugawa, K. Ohno, Y. Noda, S. Nakamura, Weakly spin-dependent band structures of antiferromagnetic perovskite $LaMO_3$ ($M = Cr, Mn, Fe$), *Journal of Physics: Condensed Matter* 30 (2018) 075502.

[58] L.-D. Yuan, Z. Wang, J.-W. Luo, A. Zunger, Prediction of low-Z collinear and noncollinear antiferromagnetic compounds having momentum-dependent spin splitting even without spin-orbit coupling, *Physical Review Materials* 5 (2021) 014409.

[59] M. Naka, Y. Motome, H. Seo, Perovskite as a spin current generator, *Physical Review B* 103 (2021) 125114.

[60] X. Chen, D. Wang, L. Li, B. Sanyal, Room temperature two-dimensional antiferromagnetic Weyl semimetal CrO with giant spin-splitting and spin-momentum locked transport, *arXiv preprint arXiv:2104.07390* (2021).

[61] K. Sheng, H.-K. Yuan, Z.-Y. Wang, Monolayer gadolinium halides, GdX_2 ($X = F, Cl, Br$): intrinsic ferrovalley materials with spontaneous spin and valley polarizations, *Physical Chemistry Chemical Physics* 24 (2022) 3865-3874.

[62] S. Feng, W. Mi, Strain and interlayer coupling tailored magnetic properties and valley splitting in layered ferrovalley $2H-VSe_2$, *Applied Surface Science* 458 (2018) 191-197.

[63] W.-Y. Tong, S.-J. Gong, X. Wan, C.-G. Duan, Concepts of ferrovalley material and

- anomalous valley Hall effect, *Nature communications* 7 (2016) 13612.
- [64] P. Jiang, L. Kang, Y.-L. Li, X. Zheng, Z. Zeng, S. Sanvito, Prediction of the two-dimensional Janus ferrovalley material LaBrI, *Physical Review B* 104.3 (2021) 035430.
- [65] P. Zhao, Y. Dai, H. Wang, B. Huang, Y. Ma, Intrinsic valley polarization and anomalous valley hall effect in single-layer 2H-FeCl₂, *ChemPhysMater* 1 (2022) 56-61.
- [66] H. Yang, M. Song, Y. Li, Y. Guo, K. Han, Ferromagnetism and valley polarization in Janus single-layer VSe, *Physica E: Low-dimensional Systems and Nanostructures* 143 (2022) 1154341.
- [67] C. Zhang, Y. Nie, S. Sanvito, A. Du, First-Principles Prediction of a Room-Temperature Ferromagnetic Janus VSe Monolayer with Piezoelectricity, Ferroelasticity, and Large Valley Polarization, *Nano Lett* 19 (2019) 1366-1370.
- [68] W. Wu, L. Wang, Y. Li, F. Zhang, L. Lin, S. Niu, D. Chenet, X. Zhang, Y. Hao, T. F. Heinz, Piezoelectricity of single-atomic-layer MoS₂ for energy conversion and piezotronics, *Nature* 514 (2014) 470-474.
- [69] S. D. Guo, X. S. Guo, X. X. Cai, B. G. Liu, Valley polarization transition driven by biaxial strain in Janus GdClF monolayer, *Phys Chem Chem Phys* 24 (2022) 715-723.
- [70] Y. Chen, J. Liu, J. Yu, Y. Guo, Q. Sun, Symmetry-breaking induced large piezoelectricity in Janus tellurene materials, *Phys Chem Chem Phys* 21 (2019) 1207-1216.

Supplementary Materials for

Multipiezo effect in altermagnetic V₂SeTeO monolayer

Yu Zhu,¹ Taikang Chen,¹ Yongchang Li,¹ Lei Qiao,¹ Xiaonan Ma,¹ Tao Hu,² Heng Gao,^{1*} and Wei Ren^{1,3‡}

¹*Department of Physics, Shanghai Key Laboratory of High Temperature Superconductors, International Centre of Quantum and Molecular Structures, Shanghai University, Shanghai 200444, China*

²*School of Materials Science and Engineering, Shanghai University, Shanghai 200444, China*

³*Zhejiang Laboratory, Hangzhou 311100, China*

[*gaoheng@shu.edu.cn](mailto:gaoheng@shu.edu.cn) [‡renwei@shu.edu.cn](mailto:renwei@shu.edu.cn)

[‡]These authors contributed equally to this work.

Table S1 The structural parameters of V₂Se₂O and V₂SeTeO monolayers: lattice constant (Å), bond length (Å) and angle (°).

System	Lattice Constant	Bond Length	Bond Angle
V ₂ Se ₂ O	a = 4.05 Å b = 4.05 Å	4.05 Å (V _{1/2} -V _{1/2}) 2.66 Å (V-Se) 2.02 Å (V-O)	99.07° (Se-V-Se) 180.00° (O-V-O) 90.00° (Se-V-O)
V ₂ SeTeO	a = 4.08 Å b = 4.08 Å	4.08 Å (V _{1/2} -V _{1/2}) 2.04 Å (V-O) 2.65 Å / 2.85 Å (V-Se/Te)	100.44° (Se-V-Se) 177.63° (O-V-O) 89.24°/90.83° (Se/Te-V-O)

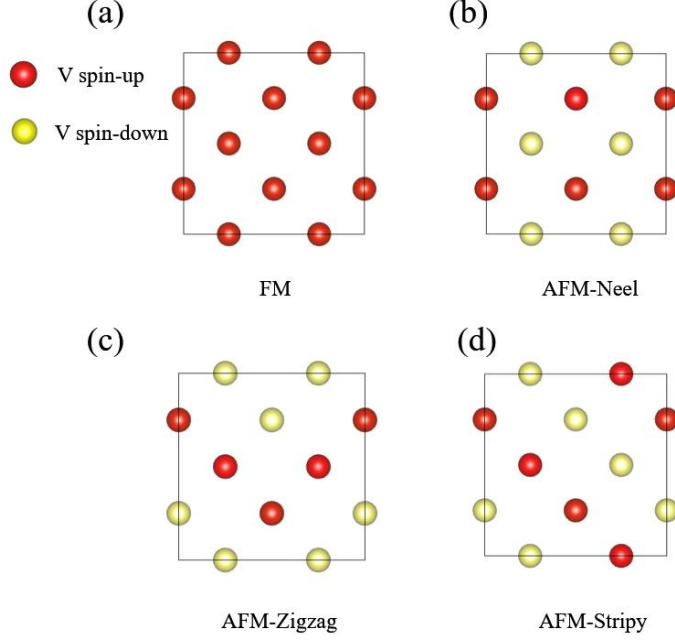


Figure S1 The initial magnetic configurations of FM and AFM for V_2SeTeO monolayer within a $2 \times 2 \times 1$ supercell.

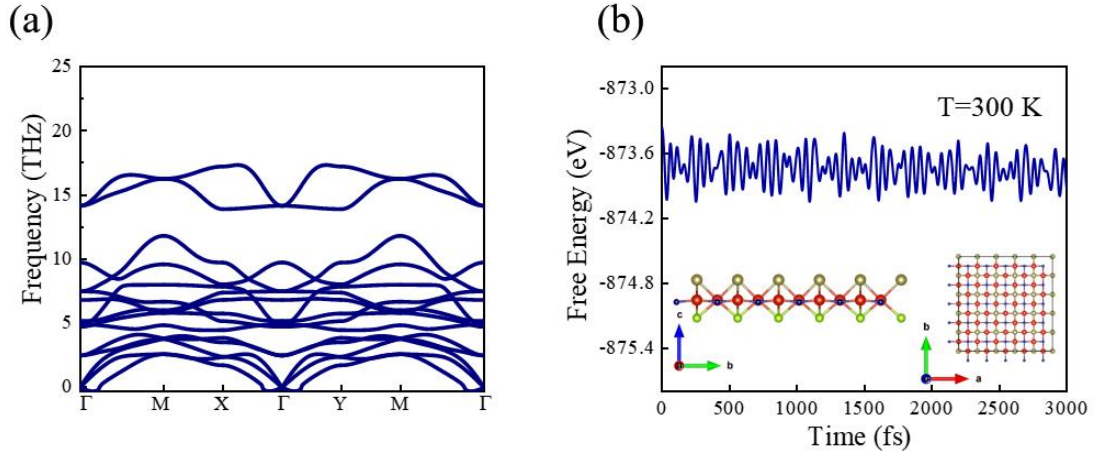


Figure S2 (a) The phonon dispersion and (b) *ab initio* molecular dynamics simulations at room temperature of V_2SeTeO monolayer.

Table S2 The PBE+U calculated elastic constants C_{ij} (N/m), relative energies (eV per V atom) for the ferromagnetic (FM) ground state and three antiferromagnetic (AFM-Neel, AFM-Zigzag and AFM-Stripy) states for V_2SeTeO monolayer.

C_{11}	C_{12}	C_{66}	$E_{AFM-Neel}$	E_{FM}	$E_{AFM-Zigzag}$	$E_{AFM-Stripy}$
114.18	18.31	36.87	0	0.18	0.13	0.22

Note S1 The details of fundamental symmetry mechanism for altermagnetic structure:

The PT symmetry (P means spatial inversion symmetry and T means time reversal symmetry) needs to be broken which protects spin degeneracy. However, this case is only applicable when considering spin-orbit coupling (SOC). When the SOC is turned off, the coupling effect of spin and spatial degrees is weakened, which means that there will be pure spin U, a spinor symmetry. The U symmetry reverses the spin and maintains momentum invariance, leading to preservation of spin degeneracy. Therefore, we need a further symmetry constraint, the UL symmetry breaking condition (U means spinor symmetry and L means translation symmetry). U reverses the spin state while L performs a translation operation on the primitive lattice, preserving the crystal structure and spin degeneracy.

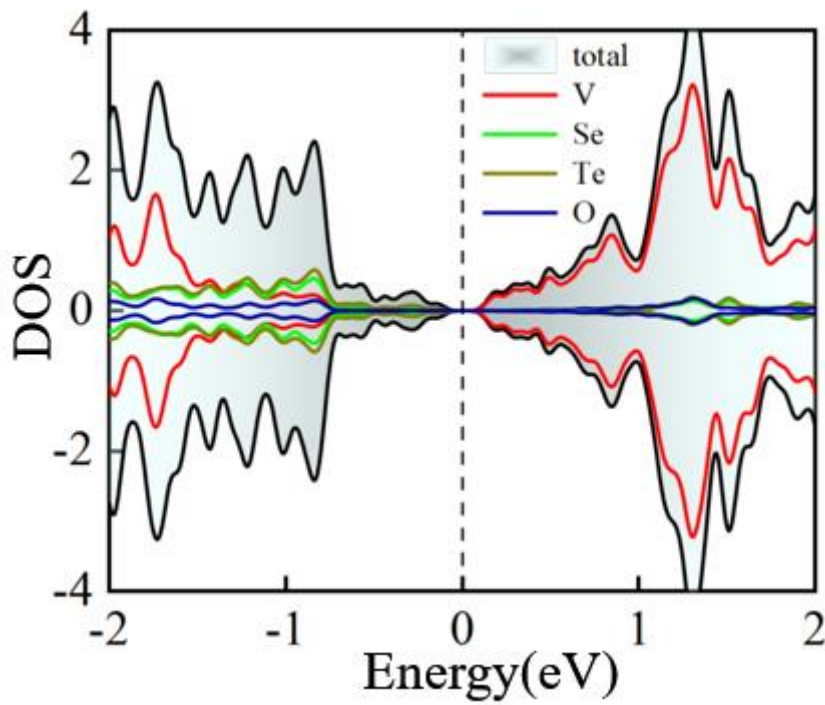


Figure S3 Partial DOS for the monolayer V₂SeTeO from PBE+U calculation.

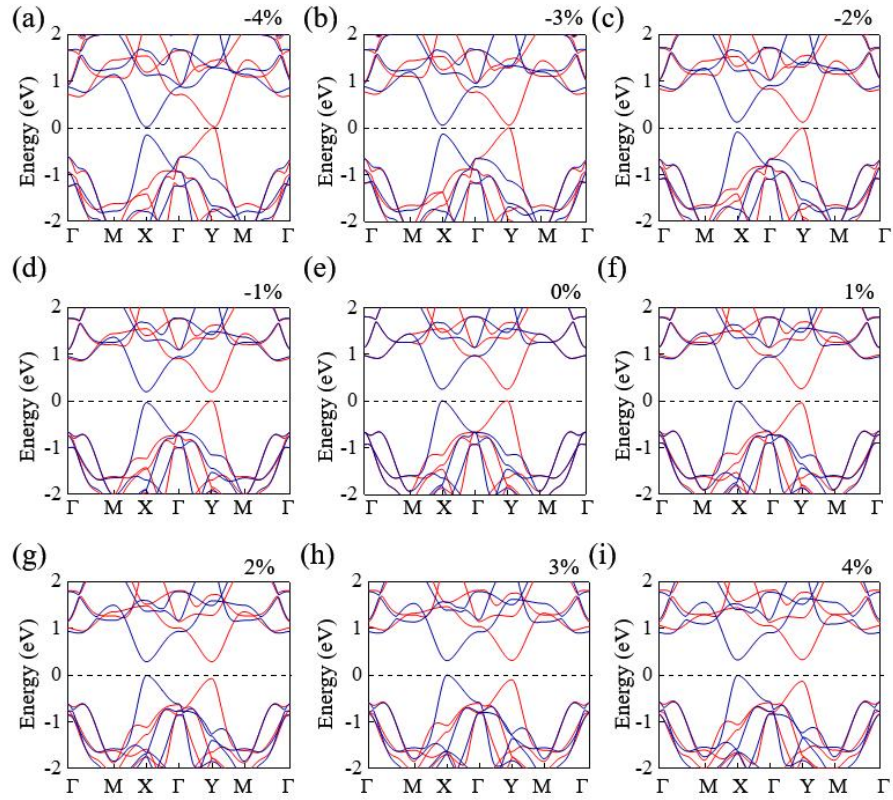


Figure S4 Spin-resolved band structures (red and blue lines for spin-up and spin-down) of the undoped V_2SeTeO monolayer under uniaxial strain along a direction from -4% to 4%.

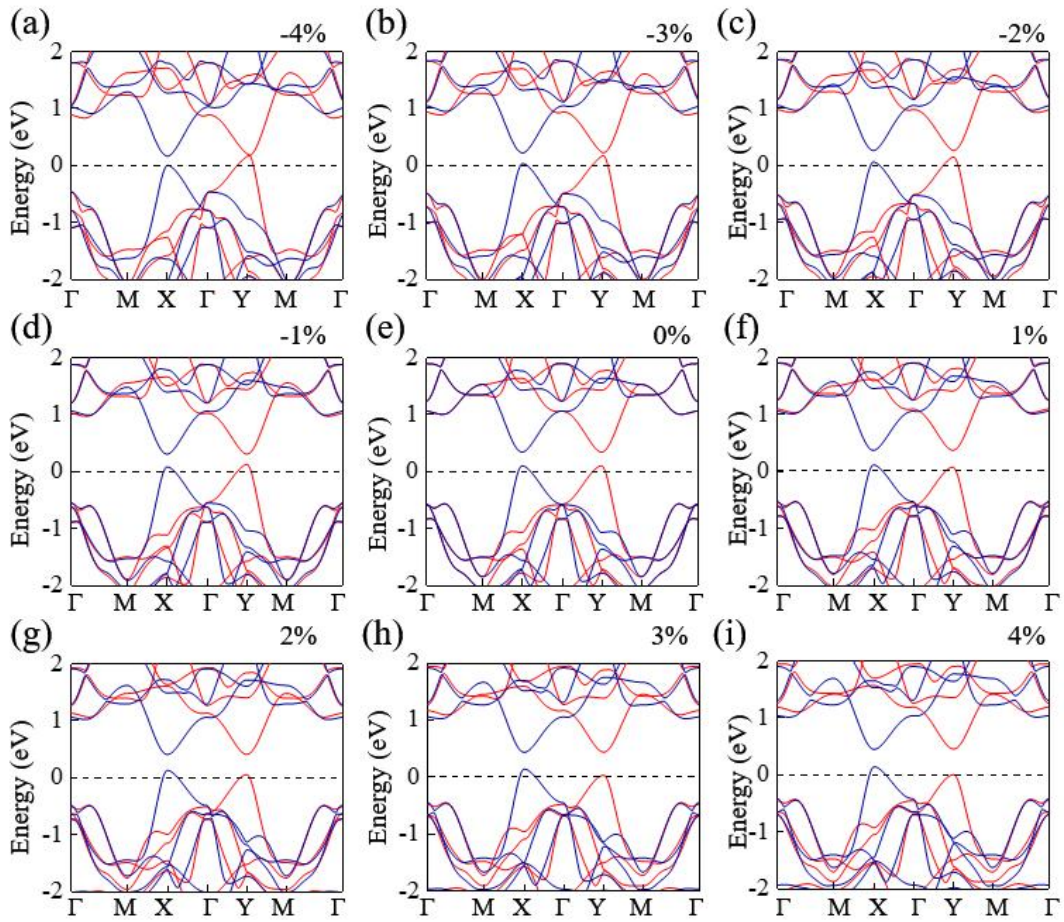


Figure S5 Spin-resolved band structures (red and blue lines for spin-up and spin-down) of monolayer V_2SeTeO with the hole doping concentration of 0.02, under uniaxial strain along a direction from -4% to 4%.